



ELSEVIER

Contents lists available at ScienceDirect

Nuclear Instruments and Methods in Physics Research A

journal homepage: www.elsevier.com/locate/nima

Latest results from the telescope array

Peter Tinyakov

Service de Physique Théorique CP225, Université Libre de Bruxelles, Blvd du Triomphe, 1050 Bruxelles, Belgium



for the Telescope Array Collaboration

ARTICLE INFO

Available online 14 November 2013

Keywords:

Ultra-high energy cosmic rays
Spectrum
Mass composition
Anisotropy

ABSTRACT

The Telescope Array ultra-high energy cosmic ray detector, situated in Utah, USA, is taking data since March 2008. We will present the latest results of the spectrum, composition and anisotropy studies based on the 4 years of the Telescope Array data.

© 2013 Elsevier B.V. All rights reserved.

1. The telescope array experiment

The Telescope Array (TA) detector is a hybrid detector of ultra-high energy cosmic rays located in the Northern hemisphere in Utah, USA (39°17'48"N, 112°54'31"W). It consists of the surface detector (SD) composed of 507 scintillator detectors covering the area of approximately 700 km² (for details see [1]). The atmosphere over the surface array is viewed by 38 fluorescence telescopes arranged in 3 stations [2], which constitute the fluorescence detector (FD) of TA.

The TA detector is fully operational starting from March 2008. In this paper we will present the results based on the analysis of the first 4 years of TA data. An update is expected soon that will include the full first 5 year of data.

The scientific goals of TA include determination of the energy spectrum of UHECR, their mass composition, and investigation of anisotropies of UHECR in the Northern sky. The ultimate purpose is to unveil the nature and origin of UHECR.

2. Data

Different subsets of the TA data are optimized for different studies. For the measurement of the spectrum of UHECR, the high quality surface detector (SD) events have been selected by the following criteria: the zenith angle $< 45^\circ$, shower core must be inside the array at a more than 1200 m from the border, number of detectors hit is 5 or larger, the quality of the reconstruction fit is $\chi^2/\text{d.o.f} < 4$, pointing direction resolution is better than 5° , the fractional uncertainty of the energy estimator $S(800)$ is less than 0.25. In the 4-year period from May 2008 until May 2012, there are 13,100 events above $10^{18.2}$ eV satisfying these criteria. The aperture of TA SD with the above cuts is 920 km² sr, while the total

exposure corresponding to this set is 3690 km² sr yr. Further details can be found in Ref. [3].

A different data set has been compiled for anisotropy studies. The idea here is to loosen the cuts in order to increase statistics, without decreasing significantly the data quality. This may be achieved by extending the zenith angle cut to $< 55^\circ$ and relaxing the border cut. This anisotropy set contains 1807 events with energies $E > 10$ EeV, 114 events with $E > 40$ EeV, and 42 events with $E > 57$ EeV.

By comparing the thrown and reconstructed arrival directions of the simulated data sets, the angular resolution of TA events with $E > 10$ EeV was found to be approximately 1.5° . Events with zenith angles between 45° and 55° have even better angular resolution. The energy resolution of the TA surface detector at $E > 10$ EeV is close to 20% [3].

In the anisotropy studies the crucial role is played by the exposure function. The exposure of the TA SD detector was calculated by the Monte-Carlo technique with the full simulation of the detector. It follows from these Monte-Carlo simulations that above 10 EeV the efficiency of the TA SD is 100%, while the exposure is indistinguishable from the geometrical one.

For the mass composition studies the stereo FD data have been used. These will be described in the corresponding section below.

3. The energy spectrum

The energy spectrum of UHECR is reconstructed from the SD data. The density of shower particles at a lateral distance of 800 m from the core, $S(800)$, is used as the energy estimator. This quantity is obtained by a lateral distribution fit, with the same functional form as used by the AGASA experiment. The energy is then estimated by using a look-up table in $S(800)$ and the zenith angle determined from an exhaustive MC simulation.

The absolute energy scale derived from the SD data alone is prone to large systematic uncertainties and possible biases associated with the modeling of hadronic interactions. On the other hand, the energy scale uncertainty is experimentally well-controlled for the FD events. We therefore correct our energy scale to the TA FD using events seen in common between the FD and SD. The observed differences between the FD and SD events are well described by a simple proportionality relationship, the SD energy scale being 27% higher than the FD. This correction is included in the spectrum shown below.

Fig. 1 shows the spectrum measured by the TA SD, where the differential flux multiplied by E^3 is shown. One can see the ankle structure and the suppression at the highest energies. A fit to a broken power law determines the energies of these features. The fit finds the ankle at an energy of $(4.6 \pm 0.3) \times 10^{18}$ eV and the suppression at $(5.4 \pm 0.6) \times 10^{19}$ eV. The power exponents for the three regions (below the ankle, between the breaks, and above the suppression) are 3.34 ± 0.04 , 2.67 ± 0.03 , and 4.6 ± 0.6 , respectively. Also shown in Fig. 1 are the spectra reported by other experiments as indicated on the plot. The HiRes and TA SD spectra agree very well, both in the energy region above $10^{18.85}$ eV where the TA SD is 100% efficient, and also at lower energies where TA employs a substantial efficiency correction.

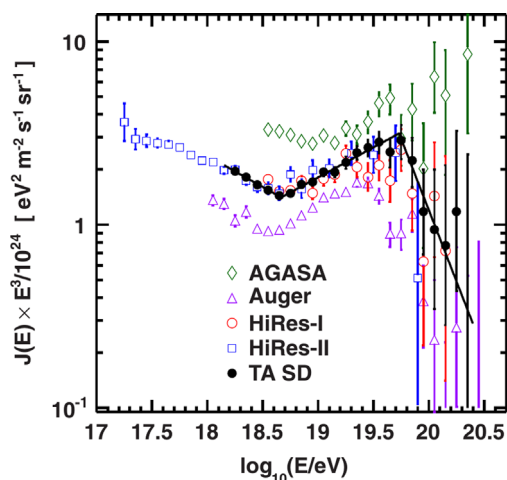


Fig. 1. TA SD energy spectrum (black points). The black lines show fit to a broken power law as described in the text. Also shown are measurements by other experiments as indicated on the plot.

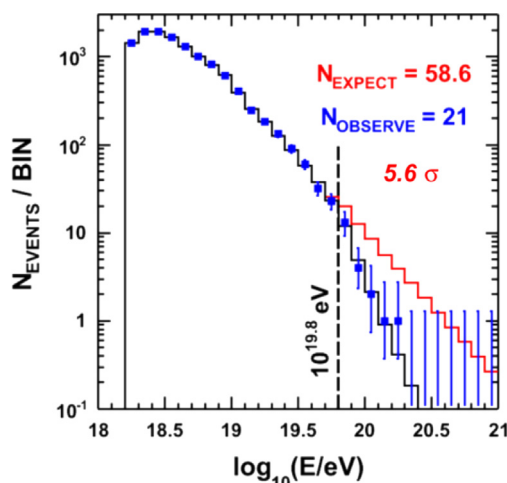


Fig. 2. Calculation of the significance of the break in the spectrum.

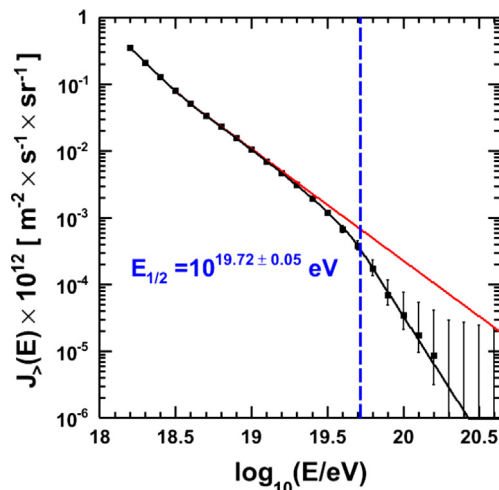


Fig. 3. $E_{1/2}$ is the energy at which the integral spectrum falls to one-half of its expected value in the absence of the cutoff.

The significance of the cutoff may be inferred by a linear extrapolation of the power law beyond the suppression point, see Fig. 2. The extrapolation predicts 58.6 events above the break, whereas TA observed only 21 events. This difference corresponds to a Poisson probability of 1.44×10^{-8} , or 5.6 standard deviations significance.

A related observable is $E_{1/2}$, the energy at which the integral spectrum falls to one-half of its expected value in the absence of the GZK cutoff (Fig. 3). This value is predicted to be $10^{19.72}$ eV for protons [4]. TA measures $\log_{10} E_{1/2} = 19.72 \pm 0.05$. Thus, the energy of the cutoff is consistent with the interpretation that the composition is protonic.

4. Mass composition

The observable sensitive to the nature of primary particle is the shower depth X_{\max} , the atmospheric depth of the maximum of the shower. This quantity can only be directly measured by the fluorescent detector, so the FD data have to be used in the composition analysis. TA stereo data is used in the present analysis. Because of the large fluctuations, the composition can only be inferred from statistical quantities such as the mean value and RMS of X_{\max} .

The expected distribution of X_{\max} was estimated by the MC shower simulation code CORSIKA. The shower library was generated using a primary energy between 10^{18} eV and 10^{20} eV. Primary particle type was taken to be protons or iron nuclei. QGSJET-I, QGSJET-II and SYBILL were used for the hadronic interaction models. The generated showers were then run through the reconstruction procedure (including the full simulation of the detector) identical to that used for the real data, in order to determine the expected X_{\max} distribution that includes all reconstruction and selection biases. In this way, the expectations for proton and iron primaries are obtained that can be compared to the real data.

Fig. 4 shows the comparison between the measured X_{\max} and that expected for proton (red lines) and iron (blue lines) in several models as indicated on the plot. The TA data are better compatible with proton composition at all, including highest energies.

In Fig. 5 we show the comparison of the observed X_{\max} distributions to those expected for proton and iron bin-by-bin in energy. Black points represent the data. Red (blue) histograms show MC simulations for protons (iron). As one can see, the

agreement is systematically better for protons than for iron primaries.

This is quantified in Fig. 6 which shows the results of the Kolmogorov–Smirnov (KS) test for each energy bin and each composition and interaction model. Low p -values indicate incompatibility of the corresponding model and the data. According to this figure, iron primaries are excluded at all except two highest energies, where the statistics is not enough to distinguish between the iron and proton compositions.

5. Anisotropy

For the anisotropy studies, a special SD data set is used as described in Section 2. To minimize the statistical penalties, we consider three high-energy subsets with energy thresholds of 10 EeV, 40 EeV and 57 EeV.

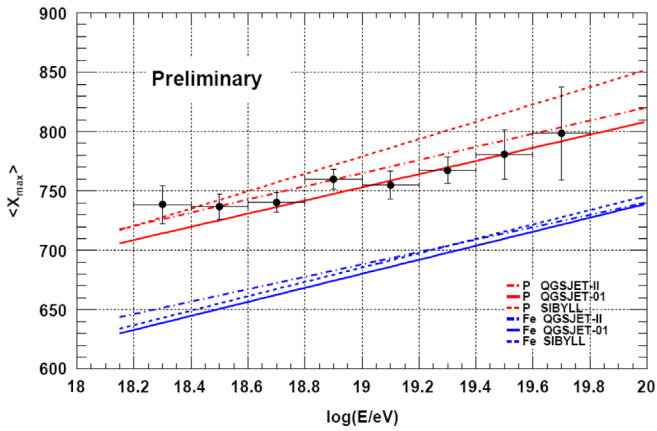


Fig. 4. The results of the X_{\max} measurement by TA (black points). Red (blue) lines show simulations in case of protons (iron) for several interaction models as indicated on the plot. (For interpretation of the references to color in this figure caption, the reader is referred to the web version of this article.)

5.1. Global distribution of the TA events

First, we examine the distributions of the TA events in the right ascension and declination in two coordinate systems: equatorial and supergalactic (SG). We generate a large (10^5) Monte-Carlo event set corresponding to the uniform UHECR distribution and compare the distribution of the right ascensions and declinations of the events in the data and in the MC set by the Kolmogorov–Smirnov (KS) test.

No significant deviations are found in the sets with the energy thresholds of 10 EeV and 40 EeV. The highest-energy set with $E > 57$ EeV shows some deviation from isotropy. The results of the KS test for this case are summarized in Table 1. The strongest deviation occurs in the supergalactic declination where the KS

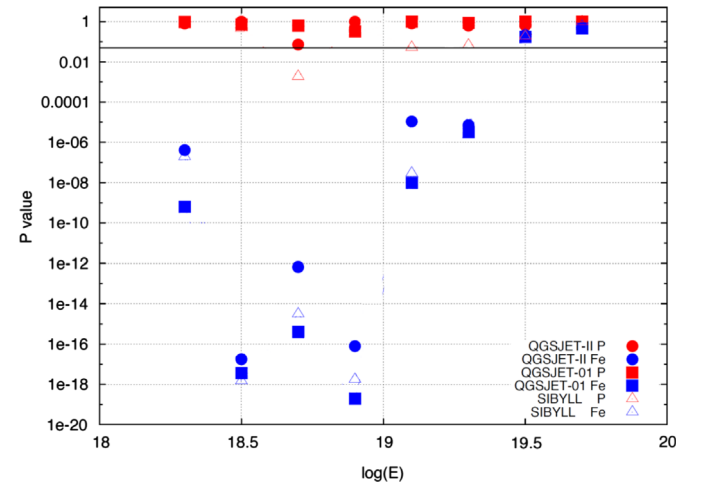


Fig. 6. The results of the KS test for compatibility between X_{\max} distributions obtained in MC simulations and the data, for two compositions (proton and iron) and different energies. Low p -values indicate incompatibility.

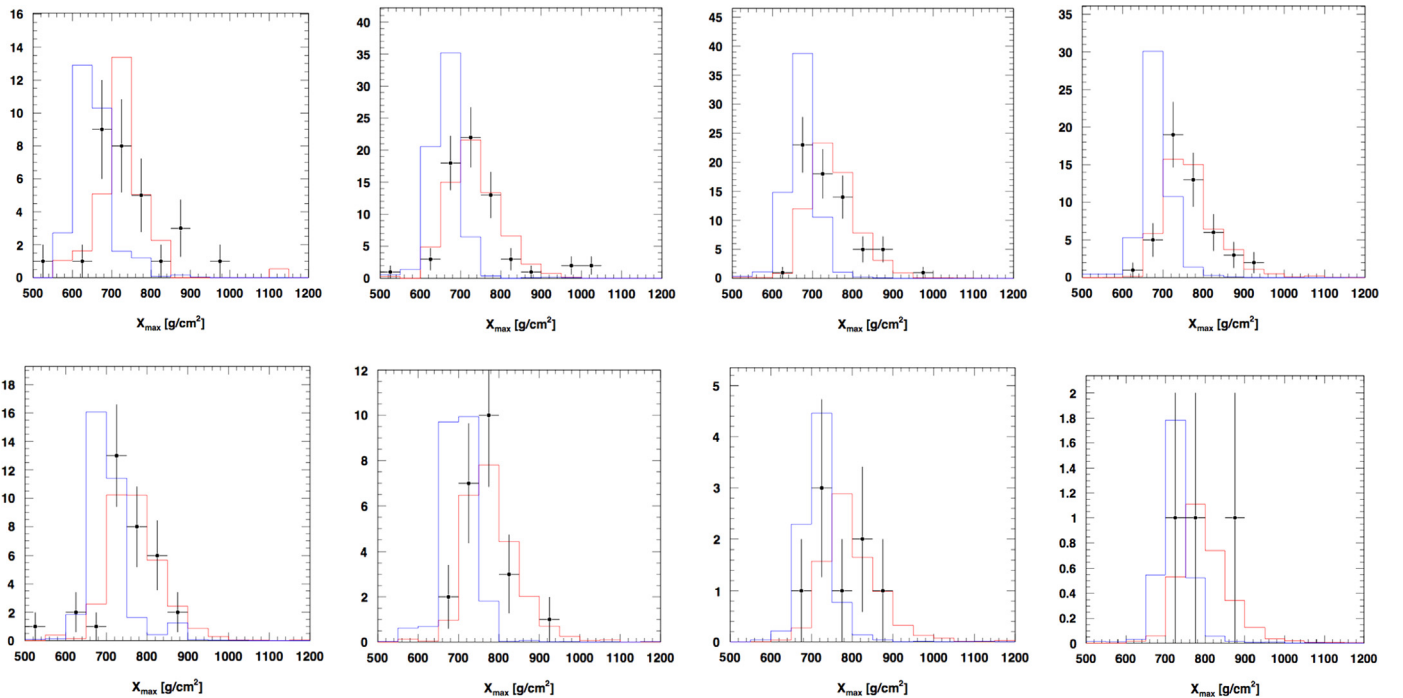


Fig. 5. X_{\max} distributions in different energy bins, from top-left to bottom-right: $18.2 < \log E < 18.4$, $18.6 < \log E < 18.8$, $18.4 < \log E < 18.6$, $18.8 < \log E < 19.0$, $19.0 < \log E < 19.2$, $19.4 < \log E < 19.6$, $19.2 < \log E < 19.4$, $19.6 < \log E < 19.8$. Red histogram: MC proton; blue histogram: MC iron. (For interpretation of the references to color in this figure caption, the reader is referred to the web version of this article.)

p -value is 0.006. The corresponding histograms are shown in Fig. 7.

5.2. Clustering and autocorrelation function

The AGASA experiment reported clustering of UHECR events with $E > 40$ EeV at the angular scale of 2.5° [5]. We repeat this analysis using the TA data set. The procedure is as follows: for a given angular separation δ we count the number of pairs of the observed events that are separated by an angular distance less than δ . We then generate a large number of random UHECR event sets, each having the same number of events as the data, and repeat pair counting in each of these sets. For each value of δ we determine the fraction of simulated sets in which the number of pairs is larger than, or equal to, the number of pairs in the data. This gives the p -value, $P(\delta)$, which describes how likely the excess of pairs, if found in the data, is to occur as a result of a fluctuation in a random set.

We treat the separation angle δ as a free parameter and determine the dependence $P(\delta)$. This test has been performed at two energy thresholds, 40 EeV and 57 EeV. The result is presented in Fig. 8 where the upper blue and the lower red lines correspond to the thresholds 40 EeV and 57 EeV, respectively. As one can see,

Table 1
Results of the comparison of the data set with $E > 57$ EeV to the uniform distribution by the KS test.

Frame	Right ascension	Declination
$E > 57$ EeV		
Equatorial	0.04	0.13
SG	0.03	0.006

there is no excess of pairs at the angular scale of 2.5° in neither of the two cases. However, there is a deviation from isotropy at angular scales of $\sim 20^\circ$ in the highest-energy data set.

5.3. Correlations with AGN

Given the catalog of putative sources, one may check whether the objects in the catalog correlate with the arrival directions of UHECRs. This can be done as follows. First, the probability p_0 is determined by the Monte-Carlo simulation that, for a given set of sources and a fixed angular separation δ , a single UHECR event falls within the angle δ from any of the sources, assuming the events are distributed uniformly. Then one counts the number n of pairs source – observed UHECR event that are separated by an angular distance less than δ . The p -value that characterizes the

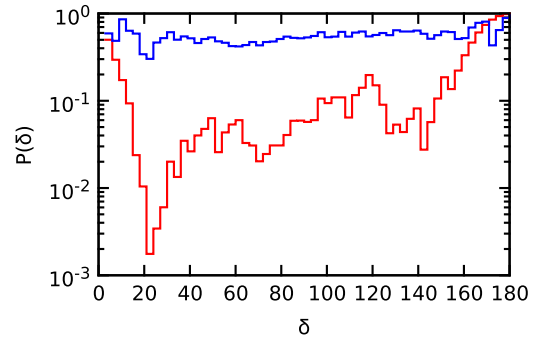


Fig. 8. The dependence of the p -value $P(\delta)$ on the pair separation angle δ for two energy thresholds: 40 EeV and 57 EeV (upper blue and lower red lines, respectively). (For interpretation of the references to color in this figure caption, the reader is referred to the web version of this article.)

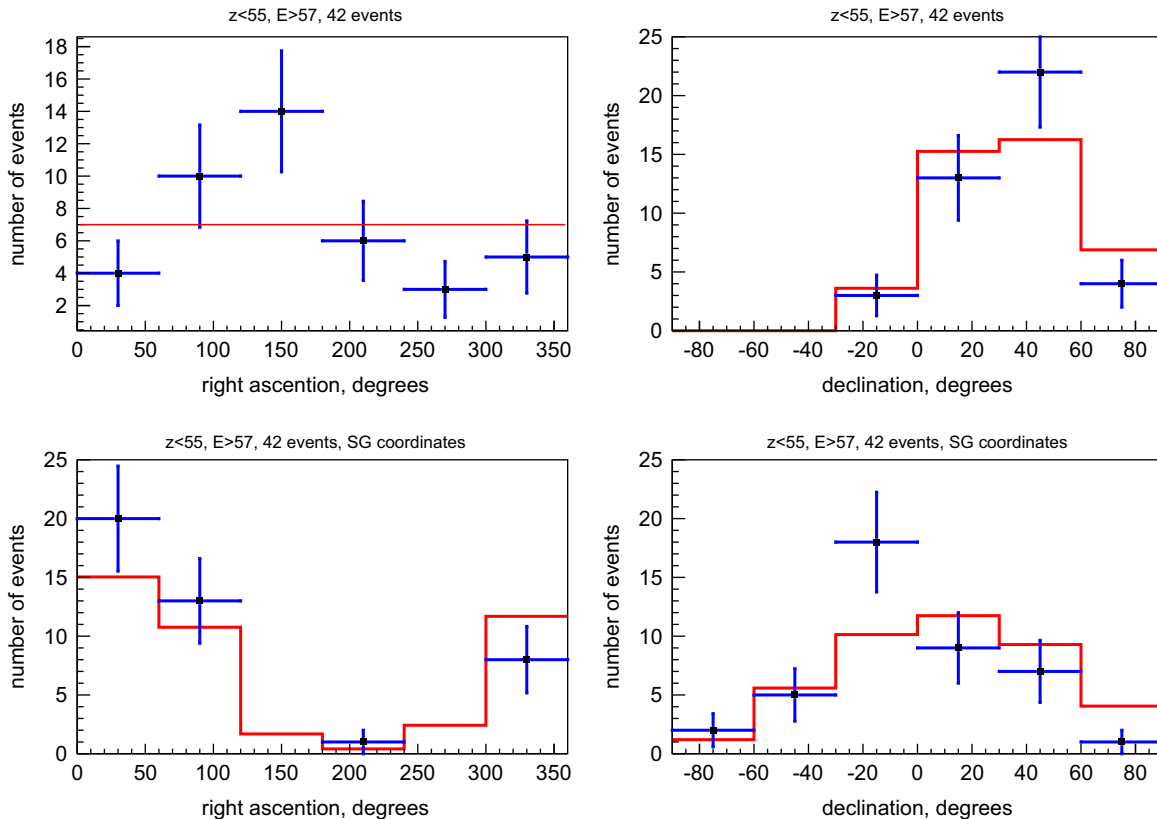


Fig. 7. Distributions of events with $E > 57$ EeV in right ascension (left column) and declination (right column) in the equatorial (top row) and supergalactic (bottom row) frames.

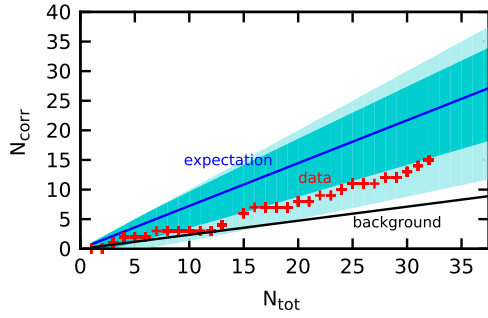


Fig. 9. The number of TA events correlating with nearby AGNs vs. total number of events.

correlation at the angular scale δ is then obtained from the cumulative binomial distribution.

We apply this formalism to the nearby AGNs from the Veron-Cetty & Veron 2006 catalog [6]. We fix the parameters following Ref. [7] as follows: $\delta = 3.1^\circ$, $E > 57$ EeV, the maximum redshift is 0.018 (465 AGNs in total). Following the previous analysis [8], we apply the zenith angle cut of 45° and tight border cuts. The evolution of the number of correlating events with the total number of events is shown in Fig. 9. With these parameters one finds $p_0 = 0.24$, while the number of correlating events corresponding to the total of $N = 32$ events is $n = 15$. This gives the p -value 0.004.

5.4. Correlation with the LSS

In the limit when the density of UHECR sources is sufficiently high so that they can be treated statistically, their distribution must follow that of the ordinary matter. The latter is inhomogeneous at scales of up to 50–100 Mpc forming the large-scale structure of the Universe (LSS). Within these assumptions, the UHECR flux can be calculated, as a function of energy, with essentially one free parameter, the typical deflection angle θ . Thus predicted flux may be compared to observations, which gives constraints on the possible values of θ . The analysis of this type has been previously performed using the HiRes [9], the PAO [10,11] and the TA [8] data. Here we present an update of this analysis using the latest TA data.

The mass distribution in the Universe was inferred from the 2MASS Galaxy Redshift Catalog (XSCz) that is derived from the 2MASS Extended Source Catalog (XSC). We have assumed that sources follow the matter distribution, and propagated UHECRs from sources to the Earth taking full account of the energy attenuation processes under the assumption that the primary particles are protons. The arrival directions were smeared with the 2d Gaussian function of the angular width θ .

The predicted flux was compared to the sky distribution of the observed UHECR events by the parameter-free flux-sampling test (see Refs. [12,8] for details). At a given value of θ , the result of the test is the p -value that shows how likely it is that the UHECR distribution follows the one expected in a given model (LSS or isotropy).

At low energies $E > 10$ EeV, the data are found to be compatible with isotropy and not compatible with the structure model unless the smearing angle is larger than $\sim 20^\circ$. This is expected, since even in the case of protons, and taking into account the regular component of the Galactic magnetic field only, the deflections of the UHECR at $E \sim 10$ EeV are expected to be of the order of 20 – 40° , depending on the direction.

At intermediate energies $E > 40$ EeV (not shown in Fig. 10) the TA data are compatible with both the isotropic distribution and with the LSS model.

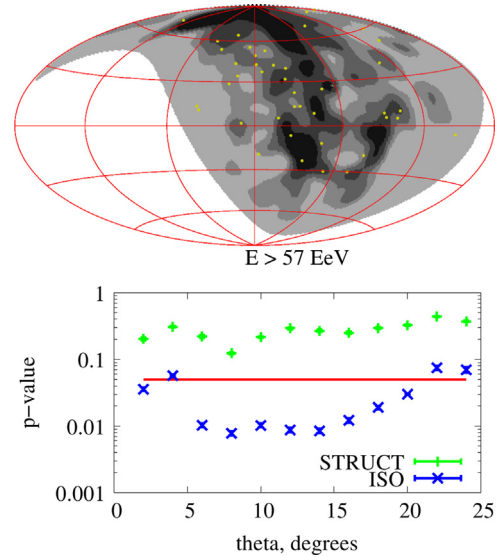


Fig. 10. Upper panel: The sky map of the TA events superimposed with the map of expected flux. The bands of grey represent the flux value; each band integrates to 1/5 of the total flux. Lower panel: p -values obtained by the flux-sampling test. The blue crosses and green pluses correspond to testing the isotropy and the LSS model, respectively. The red horizontal line shows the confidence level of 95%. (For interpretation of the references to color in this figure caption, the reader is referred to the web version of this article.)

Finally, at the highest energies $E > 57$ EeV, the behavior is different. The data are compatible with the structure model but not compatible with the isotropic distribution for most values of the smearing angle.

The results of the test at 57 EeV as a function of θ , as well as the sky map of the TA events superimposed with the map of expected flux, are shown in Fig. 10. The blue crosses and green pluses show the p -values obtained by testing the isotropy and the LSS model, respectively. The red horizontal line shows the confidence level of 95%.

6. Photon limit

Being composed of thin scintillators, the TA detectors respond equally to the muon and electromagnetic components of the extensive air shower and are therefore sensitive to showers induced by photon primaries. We use the shower front curvature as a composition-sensitive parameter. For the energy-sensitive parameter, the scintillator signal density at 800 m from the shower core is used.

The data set used in the photon limit analysis consists of the TA SD events selected by the following cuts: the distance to the boundary larger than 1200 m, the zenith angles $45^\circ < \theta < 60^\circ$, the number of scintillator detectors triggered is 7 or larger, the joint fit quality $\chi^2/\text{d.o.f.} < 5$, the reconstructed photon energy $E_\gamma > 10^{19}$ eV or $E_\gamma > 10^{19.5}$ eV depending on the energy region of interest. The details of the event reconstruction procedure are described in Ref. [13].

To estimate the flux limit, the event-by-event method [14] was used. The resulting limits based on the data collected in the period from May 2008 until May 2011 are presented in Fig. 11.

7. Summary and conclusions

We have presented the updates of the TA results concerning the spectrum, mass composition, anisotropy and the flux of

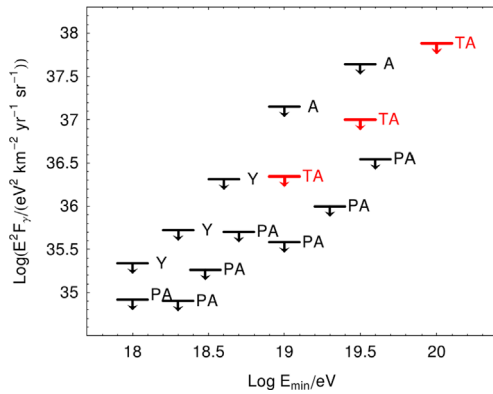


Fig. 11. The updated TA photon limit.

photons in UHECR. These updates are based on the first 4 years of the TA operation.

The spectrum of UHECR as measured by TA exhibits the ankle at 4.6 ± 0.3 EeV and the break at 54 ± 6 EeV and is fitted with a broken power law with three slopes -3.34 , -2.67 and -4.6 below the ankle, between the ankle and the break, and above the break, respectively. The significance of the cutoff at highest energies is 5.6σ . The position of the break, as well as the energy $E_{1/2}$, is compatible with the GZK cutoff and the proton composition.

The X_{\max} measurement indicates light composition compatible with protons all the way up to highest energies. No change of composition towards heavier nuclei is observed.

The sky distribution of the events is compatible with isotropic except at highest energies. Some deviation from isotropy is observed at energies $E > 57$ EeV. This deviation manifests itself in the distribution of events in the right ascension and declination in the equatorial and supergalactic coordinates, in the autocorrelation function, in the correlations with the nearby AGN, and in the correlations with the LSS. The angular scale of this deviation is ~ 20 – 30° , while its significance is still marginal, about 2 – 3σ depending on the test.

The update of the TA photon limit is also presented.

Acknowledgments

The Telescope Array experiment is supported by the Japan Society for the Promotion of Science through Grants-in-Aid for Scientific Research on Specially Promoted Research (21000002) “Extreme Phenomena in the Universe Explored by Highest Energy Cosmic Rays”, and the Inter-University Research Program of the

Institute for Cosmic Ray Research; by the U.S. National Science Foundation awards PHY-0307098, PHY-0601915, PHY-0703893, PHY-0758342, PHY-0848320, PHY-1069280, and PHY-1069286 (Utah) and PHY-0649681 (Rutgers); by the National Research Foundation of Korea (2006-0050031, 2007-0056005, 2007-0093860, 2010-0011378, 2010-0028071, R32-10130); by the Russian Academy of Sciences, RFBR grants 10-02-01406a, 11-02-01528a (INR) and 13-02-12175-ofi-m, IISN project No. 4.4502.13 and Belgian Science Policy under IUAP VII/37 (ULB). The foundations of Dr. Ezekiel R. and Edna Wattis Dumke, Willard L. Eccles and the George S. and Dolores Dore Eccles all helped with generous donations. The State of Utah supported the project through its Economic Development Board, and the University of Utah through the Office of the Vice President for Research. The experimental site became available through the cooperation of the Utah School and Institutional Trust Lands Administration (SITLA), U.S. Bureau of Land Management and the U.S. Air Force. We also wish to thank the people and the officials of Millard County, Utah, for their steadfast and warm support. We gratefully acknowledge the contributions from the technical staffs of our home institutions as well as the University of Utah Center for High Performance Computing (CHPC).

References

- [1] T. Abu-Zayyad, R. Aida, M. Allen, R. Anderson, R. Azuma, et al., Nucl. Instrum. Meth. A 689 (2012) 87, <http://dx.doi.org/10.1016/j.nima.2012.05.079> arXiv:1201.4964.
- [2] H. Tokuno, Y. Tameda, M. Takeda, K. Kadota, D. Ikeda, et al., Nucl. Instrum. Meth. A 676 (2012) 54 arXiv:1201.0002.
- [3] T. Abu-Zayyad, R. Aida, M. Allen, R. Anderson, R. Azuma, et al., Astrophys. J. 768 (2013) L1, <http://dx.doi.org/10.1088/2041-8205/768/1/L1> arXiv:1205.5067.
- [4] V. Berezhinsky, A. Gazizov, S. Grigorieva, Phys. Rev. D 74 (2006) 043005, <http://dx.doi.org/10.1103/PhysRevD.74.043005> arXiv:hep-ph/0204357.
- [5] N. Hayashida, et al., Phys. Rev. Lett. 77 (1996) 1000, <http://dx.doi.org/10.1103/PhysRevLett.77.1000>.
- [6] M.-P. Veron-Cetty, P. Veron, Astron. Astrophys. 455 (2006) 773.
- [7] J. Abraham, et al., Science 318 (2007) 938, <http://dx.doi.org/10.1126/science.1151124> arXiv:0711.2256.
- [8] T. Abu-Zayyad, R. Aida, M. Allen, R. Anderson, R. Azuma, et al., Astrophys. J. 757 (2012) 26, <http://dx.doi.org/10.1088/0004-637X/757/1/26> arXiv:1205.5984.
- [9] R. Abbasi, et al., Astrophys. J. Lett. 713 (2010) L64, <http://dx.doi.org/10.1088/2041-8205/713/1/L64> arXiv:1002.1444.
- [10] T. Kashti, E. Waxman, J. Cosmol. Astropart. Phys. 0805 (2008) 006, <http://dx.doi.org/10.1088/1475-7516/2008/05/006> arXiv:0801.4516.
- [11] F. Oikonomou, A. Connolly, F.B. Abdalla, O. Lahav, S.A. Thomas, D. Waters, E. Waxman, J. Cosmol. Astropart. Phys. 2013 (05) 015 arXiv:1207.4043, URL (<http://stacks.iop.org/1475-7516/2013/i=05/a=015>).
- [12] H.B.J. Koers, P. Tinyakov, J. Cosmol. Astropart. Phys. 0904 (2009) 003, <http://dx.doi.org/10.1088/1475-7516/2009/04/003> arXiv:0812.0860.
- [13] T. Abu-Zayyad, et al., Upper limit on the flux of photons with energies above 10^{19} eV using Telescope Array surface detector. arXiv:1304.5614.
- [14] D.S. Gorbunov, G. Rubtsov, S.V. Troitsky, Astropart. Phys. 28 (2007) 28, <http://dx.doi.org/10.1016/j.astropartphys.2007.04.003> arXiv:astro-ph/0606442.